COMPDYN 2015
5th ECCOMAS Thematic Conference on
Computational Methods in Structural Dynamics and Earthquake Engineering
M. Papadrakakis, V. Papadopoulos, V. Plevris (eds.)
Crete Island, Greece, 25–27 May 2015

OPTIMAL DESIGN FOR HIGH RESISTANT ROCKFALL BARRIERS

J.P. Escallón[1], P. Bartelt[2], and E. Chatzi[2]

[1]WSL Institute for Snow and Avalanche Research SLF and ETH Swiss Federal Institute of Technology Zurich
Flueelastrasse 11 CH-7260 Davos Dorf
e-mail: juan.escallon@slf.ch

[2] WSL Institute for Snow and Avalanche Research SLF and ETH Swiss Federal Institute of Technology Zurich
Flueelastrasse 11 CH-7260 Davos Dorf, Wolfgang-Pauli-Str. 15 CH-8093 Zürich
e-mail: {bartelt@slf.ch, chatzi@ibk.baug.ethz.ch}

Keywords: Rockfall, General Contact, Impact, Contact Interactions, Optimization.

Abstract. *Rockfall barriers are key protection systems in mountainous regions worldwide. They are composed of a netting intercepting structure connected to steel posts by means of wire-rope cables anchored to the ground. Additional energy dissipating devices can be attached to the cables. Rockfall barriers are designed to intercept and capture falling rocks with kinetic energies from 100 to about 10000 kJ. They dissipate rock kinetic impact energies by friction and plasticity. The accurate prediction of the dissipation rate, forces transmitted to the anchors and wire-net deformations depends on the approximation of contact interactions among the different structural components of the system. To treat the complex contact interactions occurring in a rockfall barrier in an efficient and accurate manner a computational scheme relying on a general contact algorithm has been developed in previous work. An issue that arises pertains to the tensile and bending coupling taking place at the connections of the chain-link netting. We considered tensile quasi-static laboratory tests to derive FE models that adequately describe such a behavior. In order to deliver a more resistant connection design, a local enhancement is proposed herein. The modified setup is optimally configured via a numerical optimization procedure and its benefits against the standard design are illustrated by means of numerical simulations. The developed modeling tools prove to comprise a versatile platform for enhancing existing designs of rockfall barriers, thereby extending the efficacy and performance of industrial solutions.*

1 INTRODUCTION

When a block or group of blocks detach from a rock face, they propagate rapidly downslope, endangering settlements and roadways. Rockfall is common problem in mountain regions worldwide, resulting in casualties and damage to infrastructure [1, 2]. Rockfall events are mitigated using either passive or active measures. Concrete shelters, rockfall dams, drapery/netting, and flexible wire-net barriers are common passive protection measures against rockfalls. These systems do not prevent the rockfall phenomenon but attempt to control the outcome. The purpose of passive measures is to dissipate the kinetic energy of rock impact by controlled plasticity and friction.

Today, the use of flexible protection systems is one of the most common rockfall protection measures [3]. These systems deform significantly to dissipate the impact kinetic energy of falling rocks. The forces transmitted to the ground are significantly smaller in comparison to rigid systems such as concrete shelters. Intercepting netting is responsible for slowing down the dissipation process. High-performance wire-netting is therefore engineered to have a non-linear response [4].

Product development in the sector of rockfall flexible systems has been carried out using a classical engineering approach. This approach is based on intuition, experience of the design engineer and extensive number of large scale experiments. As a result, product development in this sector is slow and expensive [4]. The aim of this paper is to show how an accurate FE simulation scheme in conjunction with optimization techniques can be used to develop new designs in a cost-effective manner.

Explicit Finite Element (FE) calculation schemes have been developed to simulate rockfall barriers in multi-purpose commercial codes like LS-DYNA and Abaqus [5, 6, 7, 8, 9, 10]. Initial FE simulations supported in Abaqus/Explicit [11] made use of a Contact Pairs (CP) algorithm [5]. This algorithm was able to only consider the interaction between slave nodes belonging to the wire-net truss elements and the impactor modelled as a rigid body. This approach neglected bending deformations in all structural components. Furthermore, it allowed only small relative motions of the support cables at the connections with the steel posts.

Parametric studies on similar rockfall FE models were carried out to assess several prototype modifications [6, 9]. The computational scheme was therefore developed to obtain results in a short time. This scheme neglects bending deformations and contact interactions between wire-net components. The authors approximated the real ring-net geometry by simpler geometries neglecting contact. Moreover, the sliding of the cables through the posts was roughly approximated by means of special connector elements. With these schemes GC algorithms were used under their capabilities in order to limit the computational effort. The model simplifications cause the barrier model to behave more rigidly in comparison to the real barrier. Therefore, numerically evaluated cable forces were higher and the time to achieve the impactor kinetic energy dissipation was smaller in comparison to experimentally measured values [6, 9]. Furthermore, the use of an "equivalent" numerical panel with different geometry caused the netting deformation pattern to differ from the real net. Recent FE methodologies representing contact in a more accurate manner have been implemented in LS-DYNA to model wire-nets subjected to impact [8] or rockfall barriers [10]. A FE model of a rockfall barrier with wire-rope cables and braces as part of the interception structure was implemented in LS-DYNA [10]. In this approach, a one-side contact algorithm [12] is used to treat the interactions of the impactor with the wire-netting and wire-rope cables. This algorithm only requires the definitions of the slave surface. To enforce contact properly, the slave surface needs to have a relatively fine mesh.

Moreover, the stiffer body needs to play the role of the master. Additionally, a single surface algorithm [12] was used to treat additional interactions in a rockfall barrier. This algorithm considers contact inside a slave surface list. Edge-to-edge and beam contact were considered with this approach. This model takes into account contact between rope elements of the net. The posts and impactor are modelled with solid elements. However, this modelling scheme leaded to significant unresolved penetrations. A detailed FE model of a ring-net attached to support cables that were connected to a rigid frame was accomplished [8]. In this case the impactor was a concrete spherical ball. The simulation results showed a very good match of the deformation pattern and overall stiffness.

Discrete Element (DE) calculation schemes have been developed in special-purpose codes [13, 14, 15, 16]. A pure master-slave contact algorithm was developed to treat contact between ring-net element nodes and the impact block treated as a lumped mass [14]. This algorithm was implemented in the simulation code FARO. In this code, contact is only treated for the block-net pair, which is a severe restriction. A special cable model was developed in FARO to simulate the sliding between cables and posts and wire-net and cables. The netting nodes are part of the cable macro-element. This special element allows these nodes to slide on the cable, thus creating a curtain effect [14]. In this approach, the wire ring-net is modelled as a collection of slave nodes forming a close representation of the real geometry. The nodes are then attached to each other by either purely translational springs [14] or by a combination of rotational and translational springs [13]. Chain-link elements are modelled in FARO as macro-elements in contact at the connection nodes. The tensile forces transmitted from one element to the neighbour at the connections depend on the so-called opening angle [15]. This is an approximate method to consider the influence of the bending deformations of the connections on the tensile response. The shape effects of the impact block are neglected with the contact algorithm of the FARO code. The parameters of the macro-elements and springs are calibrated using quasi-static tensile tests. Only a few parameters are needed for the calibration. However, the calibration process was still time consuming because optimization algorithms were not coupled with the model. Additional DE modelling attempts to determine the mechanical properties of wire-nets modelled with equivalent homogeneous membranes have been performed [16]. DE models have been developed to calculate double-twisted hexagonal wire-nets and to simulate rockfall kinetic energy attenuation with drapery systems. The model considers contact nodes and two types of interactions among them. The model provided good estimates for impact velocity and run-out distance [17].

This paper presents the state-of-art of a novel FE modelling scheme to simulate rockfall barriers which relies on the GC algorithm programmed in the multi-purpose code Abaqus [11]. The GC algorithm in Abaqus is two-sided, and therefore, the user does not need to define pure slave and master bodies for contact interactions, thus facilitating model generation [4]. This GC algorithm uses the penalty constraint method for explicit calculations. This method allows slight penetrations of one surface into another surface. A "spring" stiffness is applied automatically to the surfaces to resist these penetrations [11]. The "spring" stiffness is, in general, determined from stable time increment considerations and masses of the nodes involved in contact [4]. This new computational scheme was developed in order to treat the complex contact interactions occurring in a rockfall barrier in an efficient and accurate manner. The frictional contact behaviour is considered using a Coulomb-type model. The basic idea behind this scheme is to model the contact interactions between structural components as close as possible to those of real systems. Ring-net and loose chain-link rockfall systems have been already modelled with this approach [4, 18, 19, 20, 21].

Another challenge in rockfall barrier numerical modelling is, calibrating the parameters of the wire-net models. An extensive database of quasi-static tests performed on ring and chain-link nets have been collected on the course of several research projects [4, 13, 14, 15, 22]. Therefore, when a numerical model is elaborated, an inverse process needs to be performed to obtain the model parameters. This process have been carried out in the past on the basis of tedious and subjective back-calculations, which are only feasible when few parameters need to be calibrated. However, when the number of parameters constitutes an n-dimensional space as it is the case for the ring and chain-link-net models developed with this novel approach [4], the use of optimization methods becomes necessary. Mastering the use of optimization algorithms is also helpful to optimize new wire-net design as it will be shown in section 3.1.

2 STANDARD CONFIGURATION

This section presents the standard design of a chain-link net with loose connections. Moreover, it presents the standard design of a rockfall barrier where this netting typology is used. These designs have been developed by the technical department of Geobrugg AG. The features of the standard wire-netting design are presented, as well as the configuration of the prototyped rockfall barrier structure. Some aspects of the numerical models are presented. However, more complete details of the state-of-art of the simulation approach that is used are provided in [15, 18, 19, 20, 21]. In particular, a highly detailed explanation of the FE model of the chain-link netting is provided in [21], as well as details on the mode ling of the prototyped rockfall barrier structure.

2.1 Standard Chain-link net

In this particular investigation a chain-link net consisting of a three wire twisted spiral bundle was investigated [21] (Fig. 1). Each wire has a 2 mm radius (r_{wire}). The geometric dimensions of the rhomboidal mesh elements are given in Tab. 1.

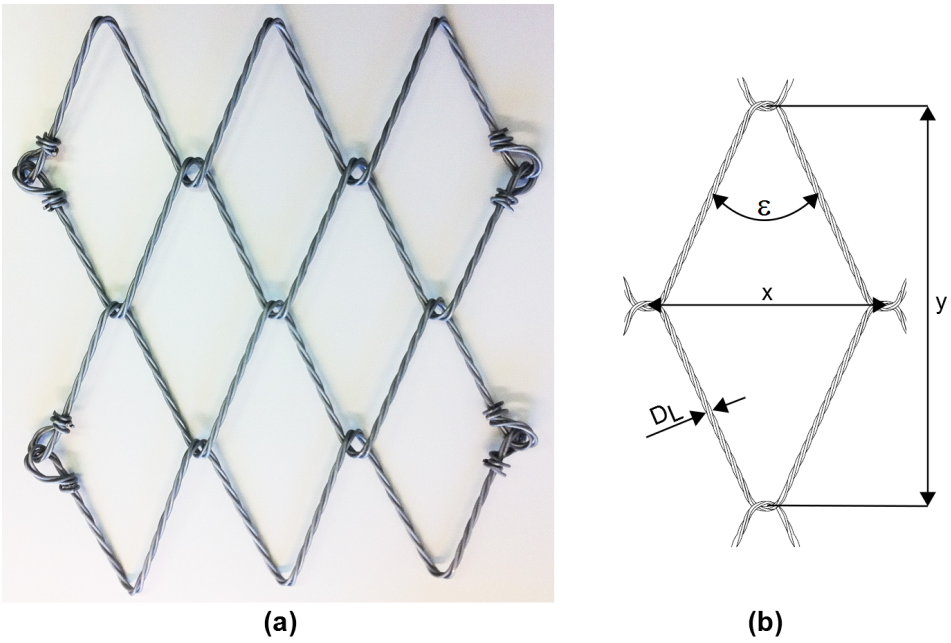

Figure 1: Triple twisted wire chain-link net components and mesh dimensions [21]

wire net producer	Geobrugg
x [mm]	180 (+/-5 %)
y [mm]	300 (+/-5 %)
mesh width D_L [mm]	8.6
mesh angle ε [degrees]	47

Table 1: Summary of the mesh characteristics and dimensions as indicated in Fig. 1 [21]

A FE model of the triple twisted wire chain-link net with loose connections was developed using the commercially available Finite Element code Abaqus/Explicit 6.14 [21]. An equivalent circular wire cross-section is obtained, which is equal to the sum of the areas of the three wires multiplied by a factor χ. This factor takes into account the fact that the cross-sectional area of the single wires is not perpendicular to the axial load, as it is the case for the simplified area [21]. Furthermore, the bending stiffness is overestimated if the area is not reduced. This approach has been applied and verified for ring net systems [18, 20]. The equivalent wire is modelled with linear elasticity, strain-hardening metal plasticity (Von Mises) and ductile damage. The numerical approach relies on the general contact algorithm of Abaqus/Explicit. The penalty method is used to approximate hard contact. Additionally, Coulomb type sliding friction is included in the contact model.

The input geometry of the chain-link elements and their connectivity is modelled according to the geometrical measurements of the real netting (Figs. 2a-b). A finer mesh is needed in the connections between chain-link elements to reproduce the axial, shear and bending behaviour obtained by the analytical chain-link model discussed in [15, 21]. Three elements in the middle of the connection are required to capture the shear transition while the remaining six elements (three to each side of the centre elements) are needed to capture the bending deformations of the connection, see Fig. 2a. These six elements were also necessary to obtain an accurate pattern of the sliding between chain-link elements. Four elements (two to each side of the centre elements) cannot correctly approximate the curved geometry of the contact zone, causing unrealistic sliding patterns between chain-link elements. Furthermore, a finer mesh having more than 9 elements per connection do not change the results significantly. Therefore, the optimal number of elements converges to 9 per connection.

The knotted connections between the ends of the chain-link elements are simplified. The connections between the border knots of the chain-link net elements are placed at the same coordinate (Fig. 2.1a). Therefore, to avoid initial over-closures [11], contact between chain-link elements is excluded in the region of the knots. Actions are transmitted from one "zig-zag" element to its neighbour at the knots by means of the so-called connector elements available in Abaqus [11]. Cartesian and Revolute connections are used to model the border "zig-zag" chain-link element connections or knots (Fig. 2.1b). The Cartesian component provides a connection between the vertices of adjacent "zig-zag" chain-link elements that allows independent behaviour in three local Cartesian directions that follow the system at the vertex a (Fig. 2.1c). Rigid behaviour is specified in the local 3-direction (z-local), while node b is allowed to change position along 1- and 2-directions (x- and y-local). The relative positions of node b with respect to node a in the local 1- and 2-directions is fixed in a working range by means of the stop option available in Abaqus/Explicit [11]. A close observation of a physical net panel reveals that the available gap for translational movement in the knotted connections is not constant. Such irregularities influence the macroscopic behaviour of the net. It is necessary to take them into account to better reproduce the soft response (stage 1) of the net panel to tensile loading (Fig. 7. In this work, the connector stop in the 1-direction is assumed to be a random number

between 5 mm and 6 mm (with a seed of 0.1 mm). A possible random variation of the gap in the 2-direction has a negligible effect on the net panel response and therefore is assumed to remain constant and equal to 6 mm. The Revolute connection type (Fig. 2.1d) is used to constrain the rotations around the 2- and 3-directions, while the 1-direction rotational component is free.

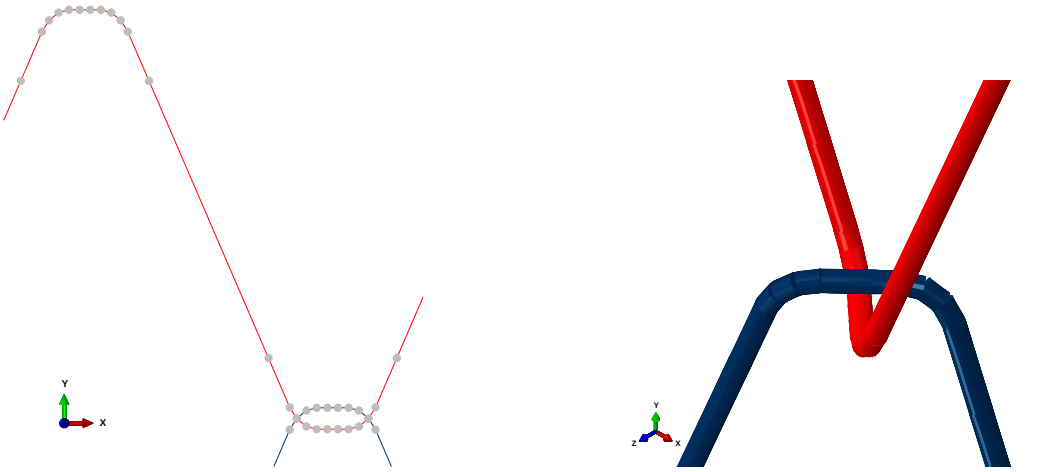

(a) element nodes

(b) connection three-dimensionality with rendered beam profiles

Figure 2: Modelling of inner connections [21].

To solve the inverse problem of finding the model parameters, a series of quasi-static tensile tests performed in the Geobrugg testing facility in Romanshorn (SG), Switzerland were considered. The tests were used to help quantify (1) the friction between the mesh elements, (2) the onset of material damage [21] and (3) the change in load eccentricity during deformation. For the quasi-static tensile tests, a rectangular net panel of 1100 x 900 mm is connected at three sides via shackles to a fixed frame (in blue Figs. 4). The upper side is connected via shackles to a moving frame (in red Figs. 4). The fixed frame is composed of steel beams which are attached to each other via bolts. The moving frame is composed of two steel plates which are attached by pins and screws. Steel sliding connections are inserted in between the frame beams and pulling machine plates. Two wire-rope cables are attached to the moving frame, which pull at a constant velocity. Prior to the test, the net is slightly pre-tensioned to avoid any possible sag. Fig. 4a shows the initial configuration of the net panel. After applying the pretension, the cables pull the moving frame at a constant velocity of 100 mm/min. The chain-link net strain rate is approximately $0.002/s$, which can be considered as quasi-static. The test machine displacement and force response of the moving frame are automatically recorded. A high-speed camera was placed above the net panel to capture the net deformation in time. Two tests were performed. Both tests lasted approximately 115 s; damage takes place only within the last 0.5 s. The pulling force reaches a peak and then drops as a consequence of damage (Fig. 4b).

To accurately model this test, true contact conditions were considered to ensure that the chain-link parameters were not influenced by significant contact simplifications. Under this approximation, the rigid and moving frames, as well as the sliders were omitted, similar to approach used in the first modelling attempts. However, in the new model, the steel pins connecting the net to the sliders were included as well as the shackles. The presence of the sliders was taken into account by constraining the movement in the z-direction of all the shackles in contact with the sliders. Furthermore, the movement in the z-direction of some beam elements

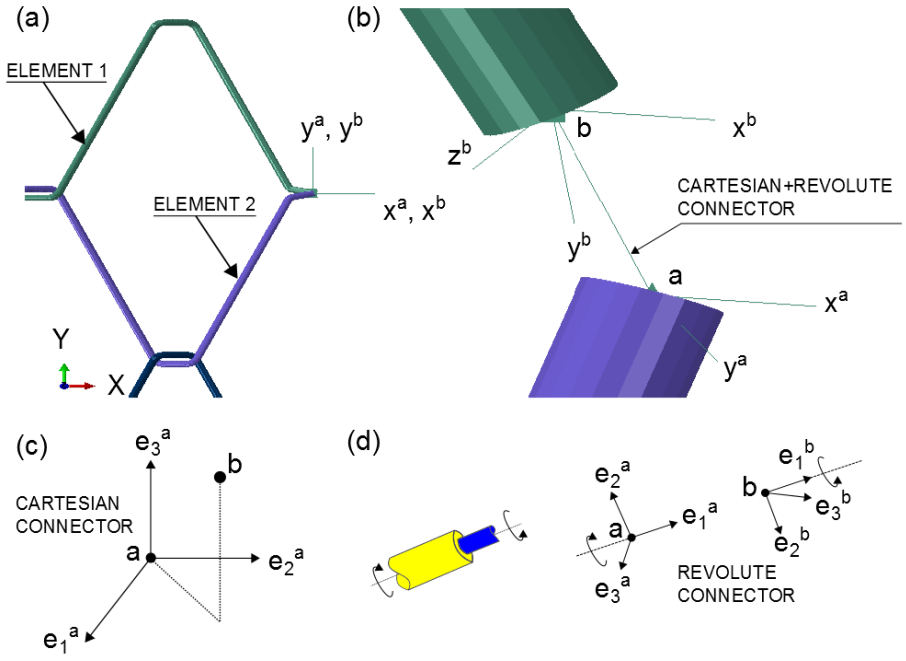

Figure 3: Modelling of the knotted connections: (a) connection type CARTESIAN, (b) connection type REVOLUTE, (c) knotted connection at the initial configuration, and (d) deformed configuration of the knot [21].

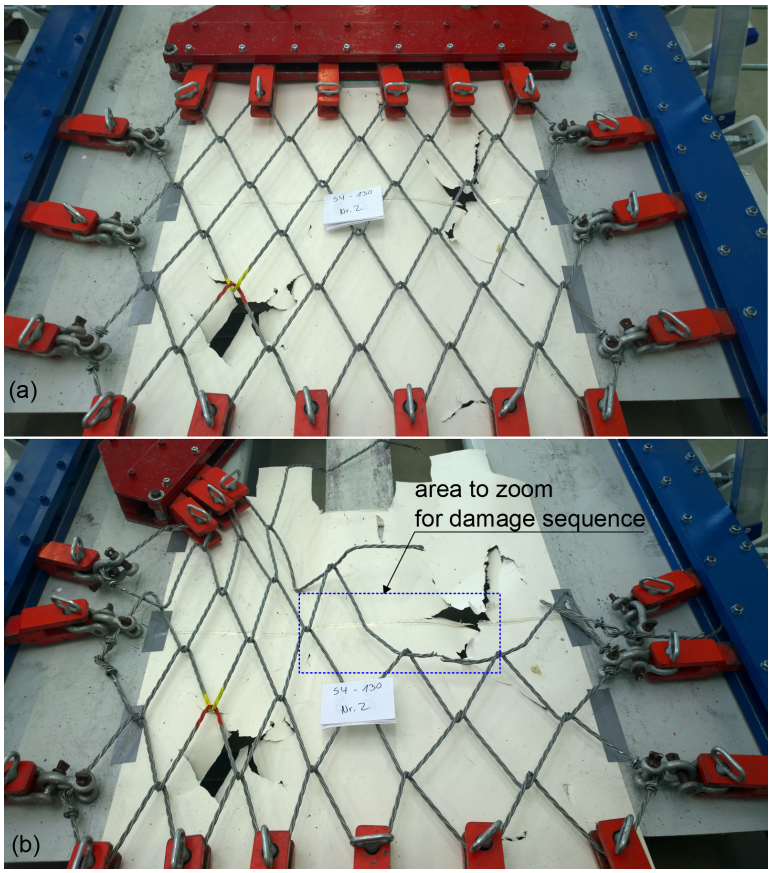

Figure 4: Tensile quasi-static test set-up [21].

was also constrained to simulate the presence of the sliders. The pins attached to the moving frame were pulled quasi-statically. Figs. 5 show the boundary conditions applied in the model. Fig. 5a shows the zones in the chain-link net were the boundary condition $UZ = 0$ was applied to take into account the movement restriction caused by the sliders. Fig. 5b shows the shackles where boundary conditions were applied, and the constrained degrees of freedom in the pins.

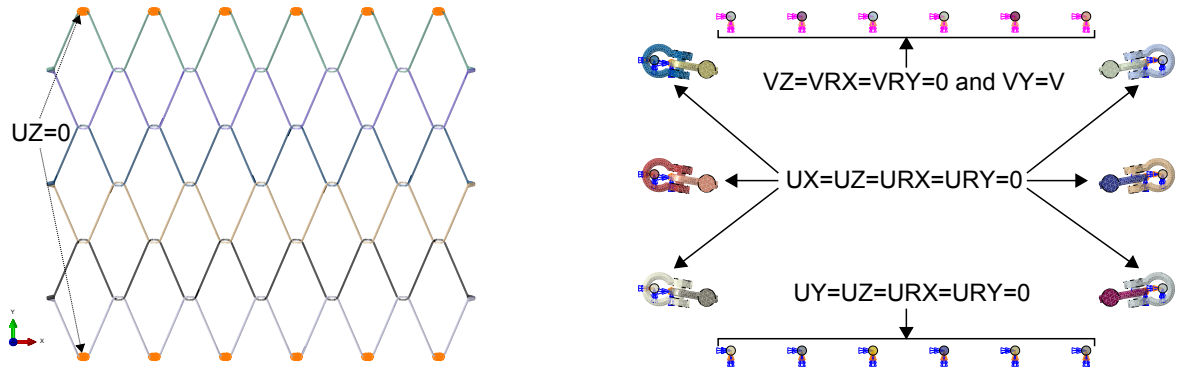

(a) applied to the net (b) applied to pins and shackles

Figure 5: Model boundary conditions [21].

The numerical simulation of the tensile test was carried out using an explicit time integration scheme. The calculation time was decreased by artificially increasing the density of the net using the mass-scaling approach [23, 24, 25]. Criteria to verify the quasi-static nature of the simulation was checked [20]. All shackles and pins were modelled as solid three dimensional rigid bodies, because they are one order of magnitude stiffer than the chain-link net. The rigid bodies were still discretized by means of finite elements, in order to have contact facets for the contact calculations.

The measured non-linear force-displacement response curves exhibit a progressive stiffening (Fig. 7) up to 100-120 mm deformation (stage 1) at which point the stiffness is approximately constant until failure (stage 2). The behaviour observed in stage 1 and 2 is a consequence of the different interaction steps between bending and axial behaviour at the connection. The details of this axial-bending interaction are provided in [15, 21]. In [21] it is shown that it is important to consider friction at the contact between chain-link elements.

To determine the best-fit parameters for the chain-link net model, a FEM based optimization scheme was implemented. The software Isight 5.9 [26] is used for this analysis due to its compatibility to the Abaqus software. The parameters to optimize in the bi-dimensional model were set as: (1) the yield curve described by two points (0, σ_y) and (ε_u^p, σ_u), (2) the Young Modulus, (3) the area reduction factor χ, and (4) the damage parameters $\overline{\varepsilon}_0^p$ (plastic strain at the onset of damage), and G_f (fracture energy per unit area). To increase the efficiency of the optimization of the model, a two stage optimization process was performed. In the first stage, damage was excluded, and to enhance the stability of the model, the ultimate plastic strain ε_u^p was assumed to be significantly large (1.5). Damage could be excluded from the first stage of the optimization since it is observed to occur at the last 0.5 sec of the 115 sec long test. The chosen objective function in this case consists in the difference between the numerical and experimental maximum force, which can be expressed as:

$$Objective\ Function = \mid F_{max,exp} - F_{max,mod} \mid \tag{1}$$

where $F_{max,exp}$ is the maximum experimental force, while $F_{max,mod}$ is the maximum force of a model optimization run. The parameters to be optimized are: (1) the equivalent wire cross-section radius $r_{section}$, (2) the elastic modulus E, (3) the yield and ultimate stresses (σ_y, σ_u). The corresponding χ factor of the chain-link net is obtained as:

$$\chi = (r_{section}/r_{wire})^2/3 \tag{2}$$

In this case the optimization surface is a smooth function. The applied scheme allowed us to use a Downhill Simplex Technique (DST), which had a fast convergence to the optimal solution [21]. For more details on the general workings of a DST one can refer to previous work by [27, 28], as well as fundamental literature on this topic [29]. Further details about the parameter optimization process are provided in [21]. Tab. 2 illustrates the optimization parameters for the chain-link net along with their lower and upper search space bounds. These bounds were defined after performing two Design of Experiments (DoEs) using the Latin Hypercube Sampling technique [30]. Finally, the optimization process is formulated as the problem of minimizing the specified objective function. Fig. 6 depicts the radial basis approximation of the objective function vs. the yield stress σ_y and the equivalent wire cross-section radius $r_{section}$. The optimization function surface is smooth and exhibits several local maxima and a region where the global minimum value is found. The simulation results of the model with the best fit parameters, served to select the plastic strain at the onset of damage $\overline{\varepsilon}_0^p$. The value of G_f allowing damage to occur at the end of the experiment was then optimized in the second stage of the optimization cycle [21]. Fig. 7 displays the results from one of the quasi-static tests and of its numerical simulation with the developed finite element model [21].

Parameter	Lower	Upper
σ_y [MPa]	1500	1700
σ_u [MPa]	2800	3000
E [MPa]	100000	110000
$r_{section}$ [mm]	2.4	2.5

Table 2: Chain-link optimization parameters (constitutive)

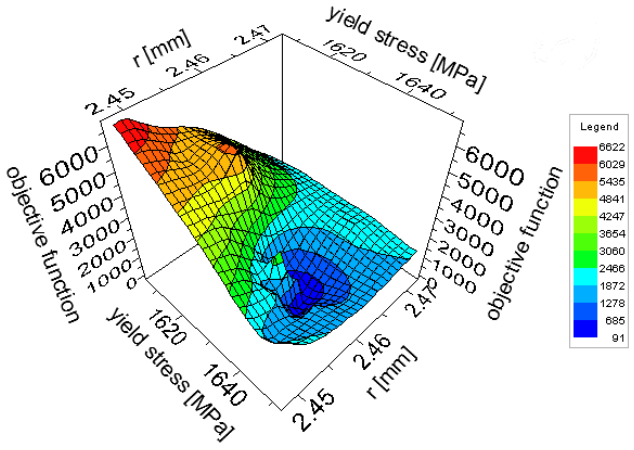

Figure 6: Radial basis function surface approximation of the objective function vs. yield stress and equivalent wire cross-section radius [21].

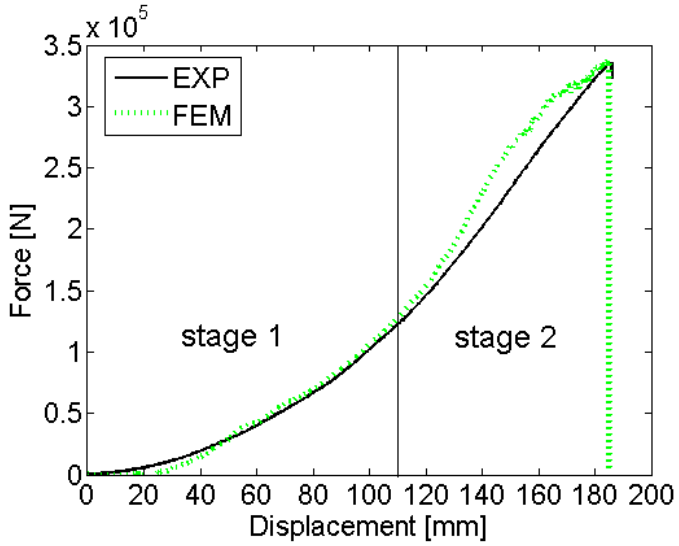

Figure 7: Force vs. displacement curve (experimental and FE simulation with optimal parameters).

2.2 Standard net-to-cables connections

The netting of a rockfall barrier able to dissipate a MEL (Maximum Energy Level) rock impact of 2000 kJ consists of loose chain-links of the typology described in the previous section. This barrier obtained the European Technical Approval according to the ETAG027 [31] guideline in 2010.

Field scale tests were performed to develop the final system. This tests revealed that when all meshes of the netting are in contact with the support cables, local failures in the chain-links take place around the posts. Therefore, through the tests an optimal solution was sought in order to avoid large stress concentrations in the netting. The final solution was to interrupt the contact between the chain-link meshes near the posts and the support cables. This is accomplished by not threading the support cables through seven meshes on each side of the inner posts and on one side of each border post (Fig. 8a). Three of the "free" meshes located on the top and bottom of the net are attached to the support cables by means of round clips (Fig. 8a-c). The round clips are made of galvanized steel wire with a diameter of 3 mm and a tensile strength of $1770 N/mm^2$. Their maximum braking force is 13760 N. The clips have negligible structural importance. All clips will fail in the case of an impact with the SEL (Serviceability Energy Level), which is approximately 700 kJ. Cable-to-net openings are created as these round clips fail progressively. The openings grow until all clips have failed. These gaps alleviate the stresses on the retaining cables and on the chain-link elements in the vicinity of the posts [21].

Full scale test data [32] was used to verify the FE model developed to simulate this barrier [21]. This rockfall fence has been modelled by using a novel computational scheme relying on a general contact algorithm [11, 21]. The hard contact behaviour is approximated by using a penalty method to enforce the contact constraint. The frictional behaviour at contact is modelled using a Coulomb-type friction [21]. Further details about the FE model of this rockfall barrier are provided in [21]. Additional features of the numerical modelling approach that has been developed to model rockfall barriers with high accuracy can be seen in [4, 19, 18, 20, 21]. The details pertaining to the test used to verify the FE model of the rockfall barrier are provided in [21]. Fig. 9 depicts the positions of the load cell as well as the anchor and energy dissipating devices in the rockfall barrier. The lateral cables (in yellow) are attached to separate anchors.

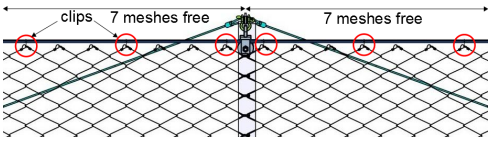

(a) free meshes rule

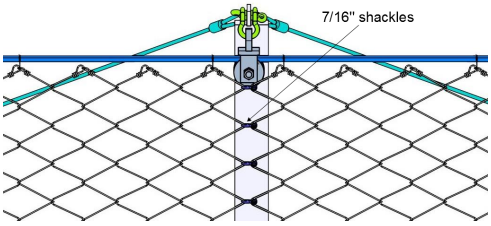

(b) connection between net panel and between net and cables (top) according to the installation kit manual

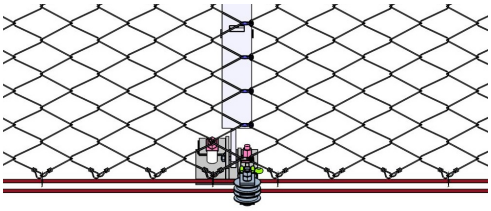

(c) connection between net panel and between net and cables (bottom) according to the installation kit manual

Figure 8: Connection of chain-link net to cables [21].

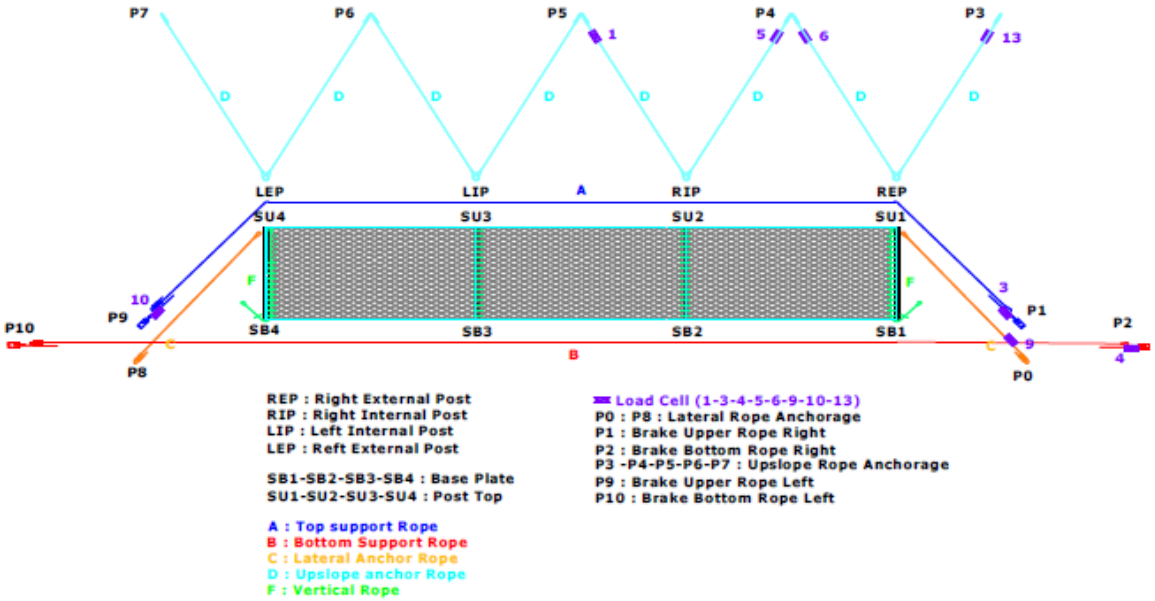

Figure 9: Load cell positions [21, 32].

Fig. 10 compares the experimental measurements (first column) and numerical simulation (second column) of the barrier during the MEL test. The third column depicts the z-location of the concrete block in the simulation. The experimental and numerical results are shown at approximately the same scale. The maximum net elongation during the MEL test (evaluated according to the ETAG No. 027) was 8960 mm, while the calculated deformation is 9013 mm. The sampling frequency of both the experimental and numerical force history data is 1/0.5 ms (2 kHz). The force histories at the load cells (MEL test) are shown in Fig. 11. The experimental force histories (dark) [32] are compared to the FEM force histories (light). Details regarding the simulation steps are provided in [21].

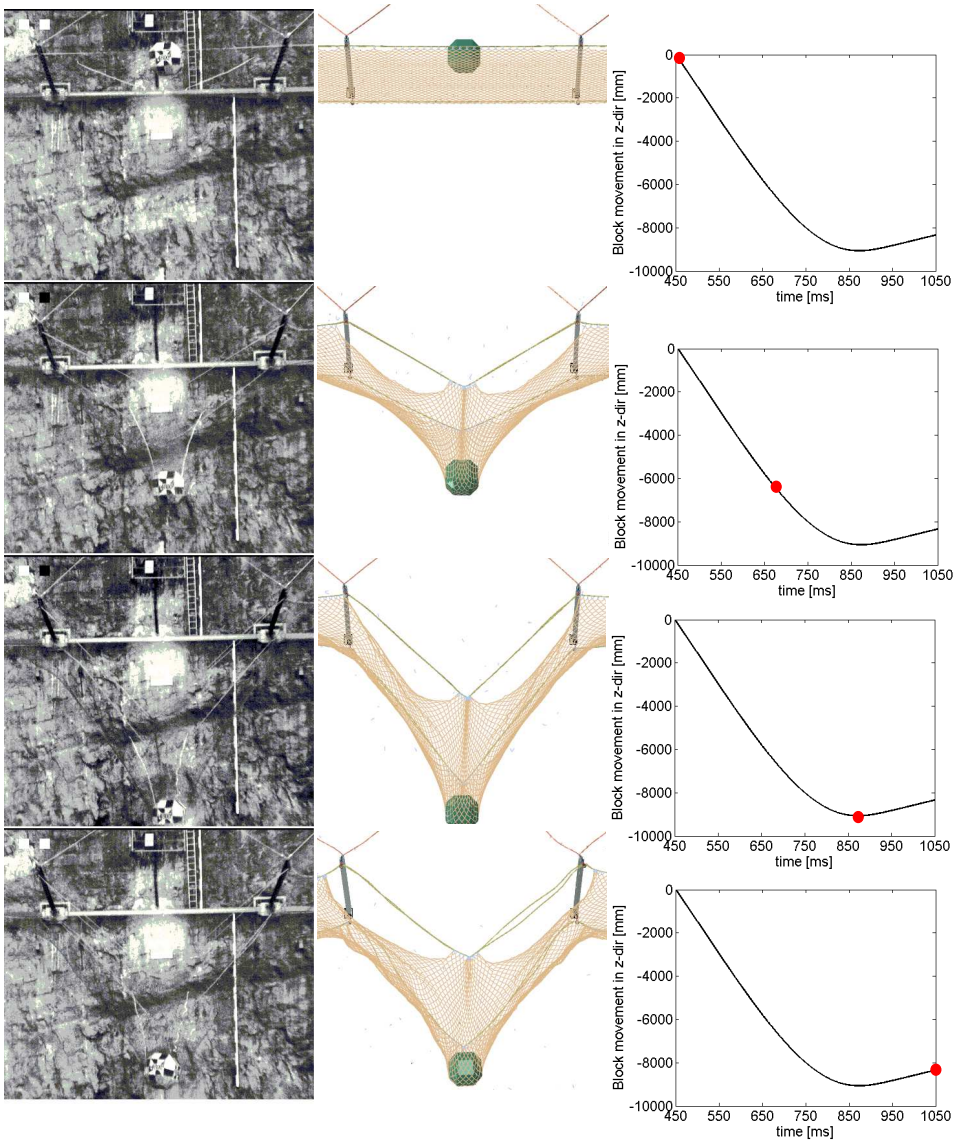

Figure 10: Experimental video frames (first column), simulation video frames (second column), and block movement evolution (third column): (a) t_1 = 0.0 ms (b) t_2 = 220 ms (c) t_3 = 420 ms and (d) t_4 = 600 ms [21].

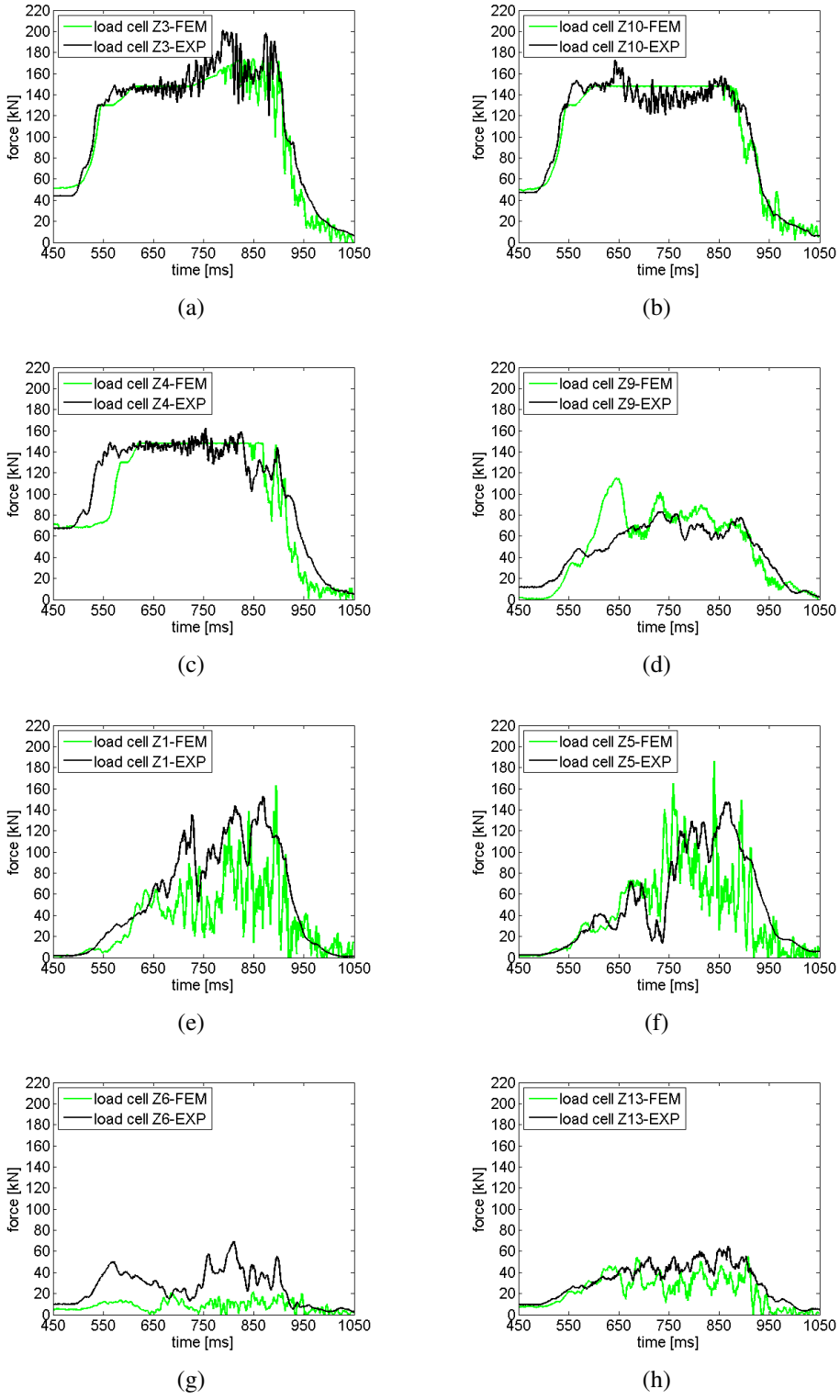

Figure 11: Load cell histories: (a-d) lateral anchors, (e-h) uphill anchors [21].

3 PROPOSED DESIGN

3.1 Optimized Chain-link net

The current chain-link net design exhibits a decrease in axial strength at the contact zones (connections). This is due to the coupling effect between axial and bending behaviour. The maximum value of the bending moment is reached at the connections and as a result the axial capacity is significantly reduced in these zones. In order to increase the axial strength at the connections, a thicker equivalent circular section can be assumed only at the contact points. The larger thickness at the connections can be assumed to be the result of two options: (1) the three wires forming the spiral bundle are thicker at the contact zones, or (2) an additional high-strength wire is winded around the three-wire bundle in a helical manner through the whole length of the connection (Fig. 12). However, in the second case, the friction between chain-links would increase with respect to the standard design. Furthermore, the thickness increase due to the additional wire would need to be determined from laboratory experiments. In this work, we will only present a simple hypothesis.

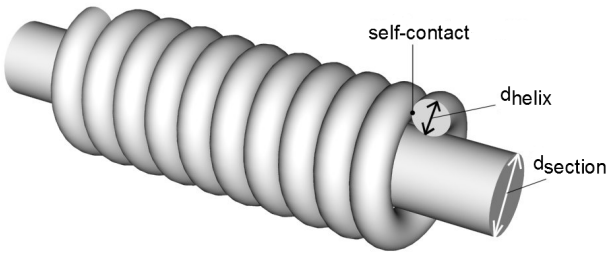

Figure 12: Helical wire wound as tightly as possible on the equivalent chain-link wire (adapted from [33]).

The increase in axial strength due to the larger section area of the equivalent wire will increase the resistance and elongation capacity of the chain-link panel. In this work, an elongation capacity increase of approximately 10% with respect to the tested standard panel is considered. Moreover, it is assumed that the strain energy of the optimized panel is the same to that of the tested panel up to the displacement at which failure occurs in the tested standard panel. The purpose of this assumption is to avoid higher forces to be transmitted to the cables in the rockfall barrier standard design (section 4.2). To fulfil this assumption regarding the strain energy, the dimensions of the three-dimensional chain-link connections need to be optimized (Fig. 13a-c).

Furthermore, if option two is chosen, the radius of the additional winded helical wire r_{helix} is optimized. In this case, the chain-link is modelled with two circular cross-sections. Namely, a cross-section that takes into account the area increase due to the winded wire along the connections (helix shape), and a cross-section that considers the calibrated area of the equivalent wire in the tested standard panel [21], which is applied to the whole chain-link except for the connections (Fig. 13c). The approximate length of the connection is:

$$L = l + f_r r_{round} \tag{3}$$

where r_{round} is equal to the radius of the round (Fig. 13b) created between the linear segments shown in Fig. 13a, and f_r is a factor that remains approximately constant for the range of variation considered for r_{round}. The length $l = (L_x^2 + L_z^2)^{0.5}$ is shown in Fig. 13a.

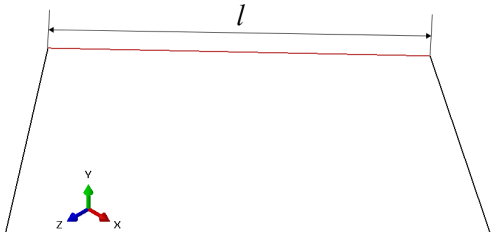

(a) connection before "create round"

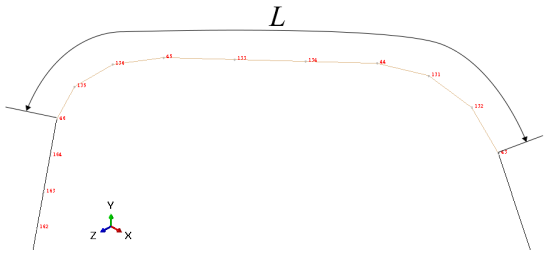

(b) finite element discretization at the connection

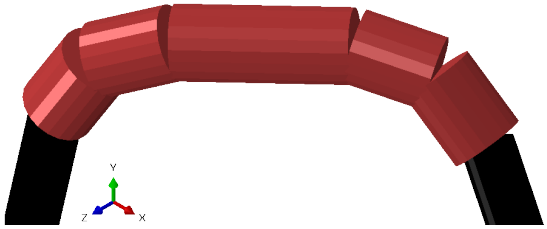

(c) rendered equivalent wire profiles

Figure 13: Connection dimensions.

The helical wire of radius a and pitch $P = 2\pi b$ is described by the following parametrisation [33]:

$$x(t) = a\cos(t), \tag{4}$$
$$y(t) = a\sin(t), \tag{5}$$
$$z(t) = bt. \tag{6}$$

Where $a = r_{helix} + r_{chain}$, and $t = N_r 2\pi$. Considering a closely packed helix (Fig. 12) [33], the pitch P is equal to $2r_{helix}$. The number of turns N_r of the helix is approximated as:

$$N_r = int(L/P) \tag{7}$$

The volume of the helical wire is equal to:

$$V_{helix} = 2\pi^2 r_{helix}^2 N_r \sqrt{(a^2 + b^2)} \tag{8}$$

The radius of the equivalent wire modelling the connection section is then assumed to be equal to:

$$R_{eq} = (r_{chain}^2 + V_{helix}/(L\pi))^{0.5} \tag{9}$$

The topology variables L_x, L_z, and r_{round} plus r_{helix} are the optimization variables of the problem. A Python script is used to generate the FE model, to calculate it using the Explicit solver and to finally produce a force-displacement curve. The Python script is parametrized, in other words, the definition of the FE model depends on the values of the optimization variables.

The Isight software is used herein to quantify how fit a candidate solution is, i.e., how closely it approximates the sought quantities. The first quantity is a desired force-displacement curve. The optimization function to be minimized is then, the absolute area difference between the sought and simulation curves (Fig. 14). The second quantity is the peak force, which is to be maximized, then constituting a second optimization function. The multi-objective function problem is posed as a single objective by combining both optimization functions into one, where the resulting function is to be minimized:

$$f_{opt} = f_{w1} f_1 - f_{w2} f_2 \tag{10}$$

where f_{w1} and f_{w2} are the weight factors. In this case an equal weight was given to both functions and therefore $f_{w1} = f_{w2} = 1.0$.

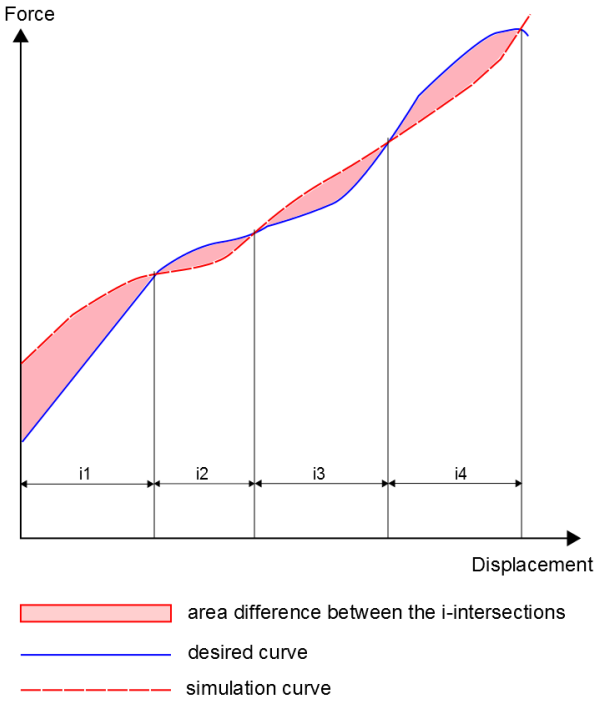

Figure 14: Area difference to be minimized (optimization function 1).

Tab. 3 illustrates the optimization parameters for the chain-link net along with their lower and upper search space bounds. Finally, the optimization process is formulated as the problem of minimizing the specified objective function. The process to obtain the lower and upper bounds of the optimization variables, as long as the details of the solution of a similar optimization problem are provided in [20]. Figure 15 depicts the radial basis approximation of the composed objective function vs. the connection dimensions L_x and L_z. This figure reveals a multi-modal optimization problem. The optimal values of L_x and L_z are approximately 29 mm and 26 mm respectively. These values are larger than those used to model the standard netting design which are: 25 mm and 23 mm respectively. Therefore, in case of using a thicker cross-section (either just at the connection or globally), the optimal solution is to also increase the connection length.

Parameter	Lower	Upper
L_x [mm]	25.0	31.0
L_z [mm]	24.0	28.0
r_{round} [mm]	11.0	13.0
r_{helix} [mm]	1.0	2.0

Table 3: Chain-link optimization parameters (topology and contact equivalent wire section)

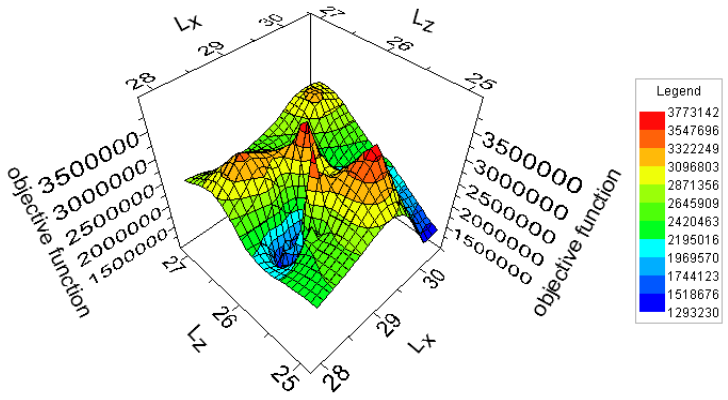

Figure 15: Radial basis function surface approximation of f_{opt} vs. L_x and L_z.

3.2 Net-to-cable connection modifications

The higher resistance achieved by the new chain-link netting design is useful to perform modifications aimed to improve the performance of the rockfall barrier system already discussed. The only modification considered in this work was to reduce the number of "free" meshes from seven to six per post side (Fig. 16). The scheme used to connect the chain-link netting to the support cables is explained in detail in [21]. Basically, there are two types of modelled clips connecting the netting to the support cables: (1) rigid body [11] type clips which by definition cannot fail. They are used in the locations where in the real barrier, the cables are threaded through the netting. Large scale tests have shown that failures do not occur in this type of connection, and therefore assuming rigid body type clips is acceptable [21]; and (2) deformable type clips modelled with metal plasticity and a ductile damage law [21]. These clips represent the realistic clips that connect some of the "free" meshes to the support cables. The clips that fail are highlighted in Fig. 16. The purpose of the implemented modification is to reduce the netting deformation. This is useful in locations where the space allowed for the netting deformation is limited.

Figs. 17a-b shows the deformed state of the modified barrier at two different times (with the same scale), namely: the time where the maximum deformation is achieved (Fig. 17a), and the time where the maximum deformation was achieved in the standard design (Fig. 17b). The maximum deformation of the proposed design with the optimal chain-link netting is 6330 mm, that is 2630 mm. Therefore, the deformation space of the system with the proposed modification is reduced by more than 2 meters. Fig. 17a shows that 3 deformable clips (type 2) did not fail. This fact caused an antisymmetry effect on the model and therefore the impactor takes an inclined direction. Those clips did not fail because the forces transmitted to the support cables are reduced in the modified design. This is because the energy dissipating devices (brakes) connected to the support cables dissipate less energy with the proposed design. The brakes

experience a smaller sliding in comparison to the standard design case. The larger frictional dissipation of the optimal netting compensates the lower energy dissipation of the brakes.

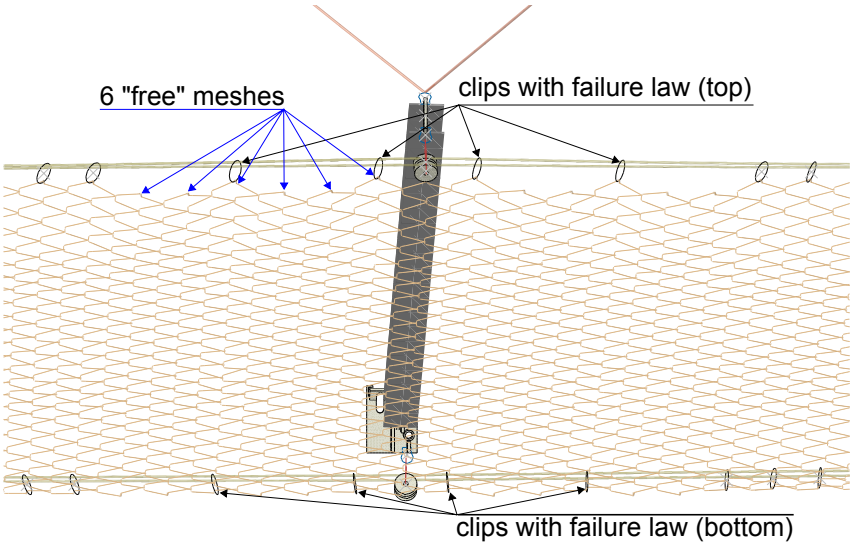

Figure 16: Connection of chain-link net to cables with 6 "free" meshes by post side (bottom and top).

4 COMPARATIVE PERFORMANCE OF PROPOSED VS. STANDARD APPROACH

4.1 Chain-link panel

Fig. 18 illustrate the comparison between the simulation results of the standard and optimal chain-link netting design. It can be observed that the modified net has an increase of $\approx 10\%$ in elongation capacity and of $\approx 5\%$ in strength. It is also observed how the strain energy of both curves is similar up to the force-elongation point where failure occurs in the standard design. This in fact is a result of the optimization goal expressed by means of the multi-objective optimization.

4.2 Rockfall barrier

Fig. 19 illustrate the comparison between the simulation results of the standard and modified 2000 kJ rockfall barrier design. It can be observed how the forces decay faster in the modified design because of the smaller brake time. Until the decay time (about 750 ms) the forces in the modified system are slightly larger in comparison to the forces in the standard system. Therefore, it is proved that the optimal netting does not transmit forces that are significantly larger than those transmitted by the standard chain-link netting.

5 DISCUSSION

The solution of a topology optimization problem of a wire-net approximated by an equivalent circular section and discretized by beams elements can be obtained by means of simple algorithms such as the Downhill Simplex (DS) [29]. On the other hand, when the shape of cross-section is not knowing a priori, a three dimensional element discretization of the structural component is needed and the optimal cross-section shape and area is found by means of more complex numerical procedures such as the SIMP (Solid Isotropic Material with Penaliza-

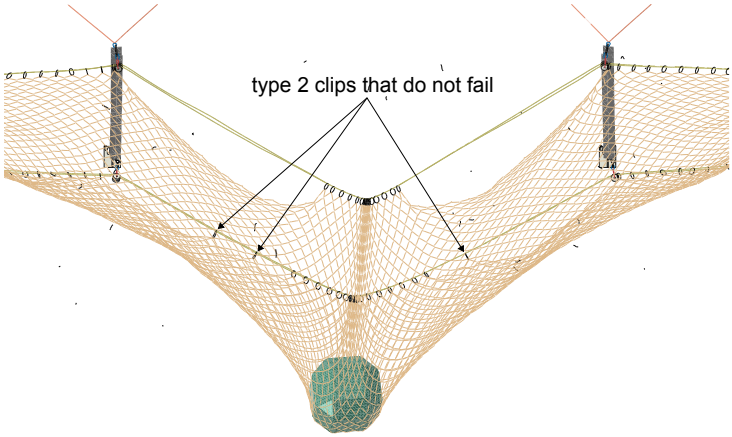

(a) Maximum deformation of the proposed design

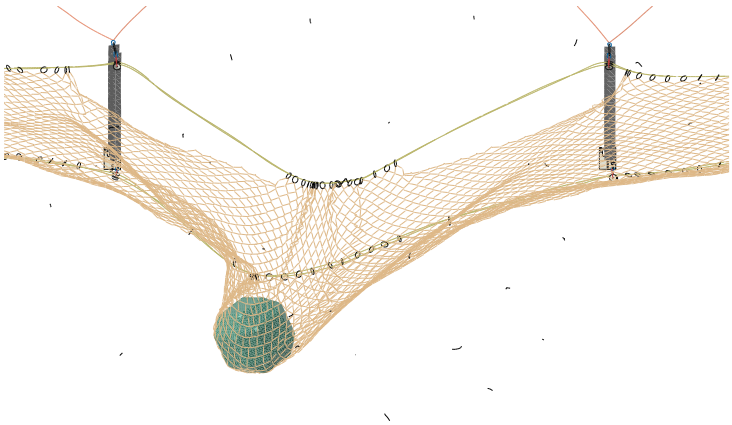

(b) Deformation of the barrier at the time where the standard design achieves the maximum deformation

Figure 17: Simulation video frames: (a) t_1 = 260 ms and (b) t_2 = 420 ms.

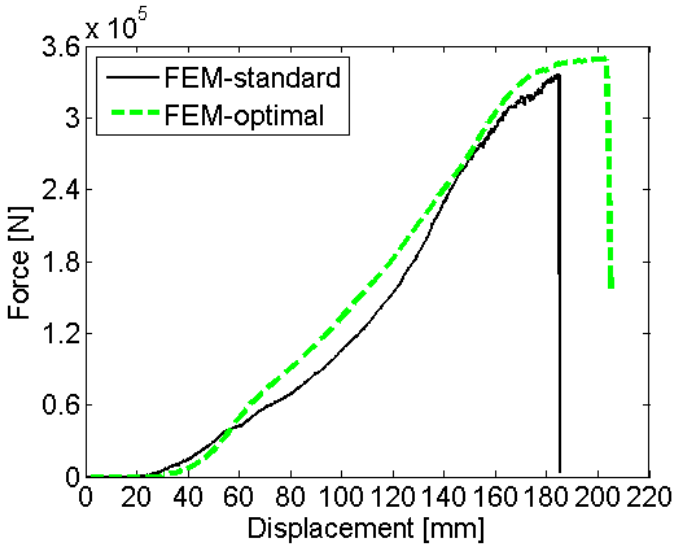

Figure 18: Force vs. displacement curve from FE simulations (standard and optimal designs).

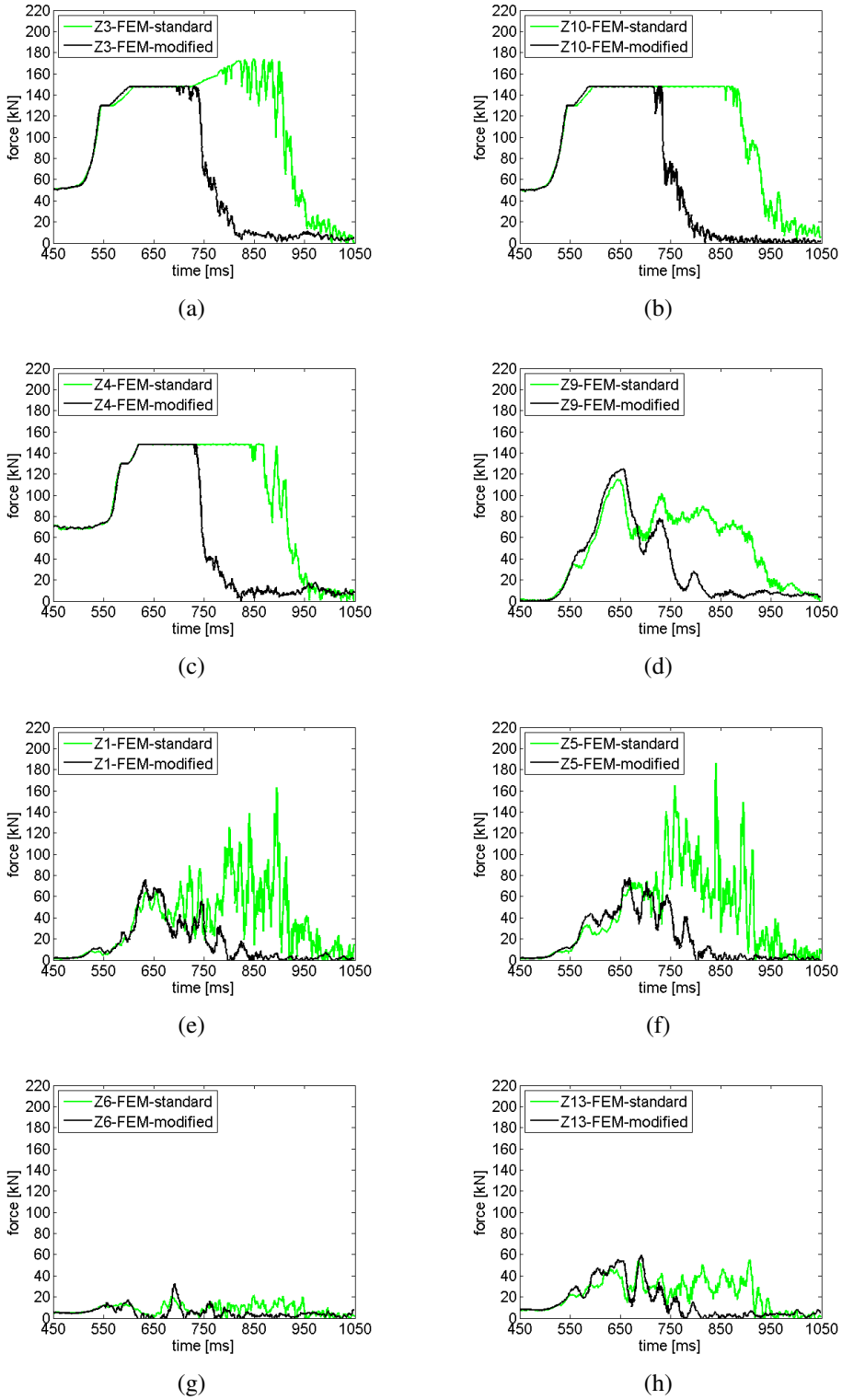

Figure 19: Comparison between the simulation results of the standard and modified 2000 kJ barrier: (a-d) lateral anchors, (e-h) uphill anchors.

tion) approach [34]. For structures subjected to impact, topology optimization problems can be solved with the Hybrid Cellular Automata (HCA) [35] or the Equivalent Static Load (ESL) [36, 37] method. The objective in the impact case is to maximize the internal energy.

Rockfall barrier developers should advance in the design of more efficient energy dissipating devices with larger absorption capacities. In order to optimize new designs, methods such as the HCA and ESL can be used. Software such as Tosca [38] based on standard FE software (Abaqus, ANSYS, MSC Nastran) is used to perform shape and topology optimization of structures under static and dynamic loading. Additionally, LS-TaDSC [39] can be coupled with LS-DYNA to also solve topology optimization problems involving large non-linearities, dynamic loads and contact conditions. Another component where topology optimization would be interesting for cutting costs, is the ground plates. The FE modelling aspects of standard ground plates and their connection with the posts can be seen in [20, 21].

This paper presents an example of how topology optimization can be useful to obtain better performing systems. Rockfall barriers can be therefore optimized using existing methods. In order to speed up product development and to cut costs, the rockfall barrier developers would benefit from an analytical/numerical approach to optimize their designs such as it is already the norm in other industrial sectors [40, 41, 42, 43, 44]. The re-configured design for large scale experiments (after optimization) is already close to optimum [45].

In the structural optimization of the chain-link netting, assumptions regarding the equivalent wire at the connections and the friction coefficient between the modified chain-links were made. In order to validate the results of the simulation, real scale tests need to be performed.

6 CONCLUSIONS

We make the following conclusions:

- Topology optimization of standard netting designs can be carried out using the same techniques already employed to optimize the parameters of the netting FE models.
- Optimized existing wire nets can allow modifications to standard designs aimed to enhance their performance in terms of energy dissipation and barrier elongation.
- Topology optimization of completely new netting designs can also be performed. However, it is first necessary to obtain the equivalent circular cross-section as it has done for ring and chain-link nets [20, 21].
- More advanced methods such as the HCA and ESL are necessary to perform topology optimization of better performing energy dissipating devices. In these cases a 3D model of the brakes and a three-dimensional finite element discretization is necessary.
- New ground plates including dissipation capabilities can also be subjected to topology optimization. Such components will reduce the forces transmitted to the ground, causing the installation costs of the rockfall barriers to be reduced.

REFERENCES

[1] F. Guzzetti, P. Reichenbach, and G. F. Wieczorek. Rockfall hazard and risk assessment in the yosemite valley, california, usa. *Natural Hazards and Earth System Science*, 3(6):491–503, 2003.

[2] F. Agliardi, G. B. Crosta, and P. Frattini. Integrating rockfall risk assessment and countermeasure design by 3d modelling techniques. *Natural Hazards and Earth System Science*, 9(4):1059–1073, 2009.

[3] A. Volkwein, K. Schellenberg, V. Labiouse, F. Agliardi, F. Berger, F. Bourrier, L. K. A. Dorren, W. Gerber, and M. Jaboyedoff. Rockfall characterisation and structural protection - a review. *Natural Hazards and Earth System Science*, 11(9):2617–2651, 2011.

[4] Juan Pablo Escallón Osorio. *Simulation of flexible steel wire-net rock-fall barriers via finite element model updating*. PhD thesis, ETH, 2015.

[5] A. Cazzani, L. Mongiovì, and T. Frenez. Dynamic finite element analysis of interceptive devices for falling rocks. *International Journal of Rock Mechanics and Mining Sciences*, 39(3):303 – 321, 2002.

[6] Cristina Gentilini, Laura Govoni, Stefano de Miranda, Guido Gottardi, and Francesco Ubertini. Three-dimensional numerical modelling of falling rock protection barriers. *Computers and Geotechnics*, 44(0):58 – 72, 2012.

[7] M. Spadari, A. Giacomini, O. Buzzi, and J.P. Hambleton. Prediction of the bullet effect for rockfall barriers: a scaling approach. *Rock Mechanics and Rock Engineering*, 45(2):131–144, 2012.

[8] J. Yiu, Y. Huang, J. Pappin, S.H. Julian, Kwan, and K.S. Ho. Ken. Landslide mobility and flexible barrier numerical modeling using ls-dyna. In *12th International LS-DYNA Users Conference*, 2012.

[9] C. Gentilini, G. Gottardi, L. Govoni, A. Mentani, and F. Ubertini. Design of falling rock protection barriers using numerical models. *Engineering Structures*, 50(0):96 – 106, 2013.

[10] Phuc Van Tran, Koji Maegawa, and Saiji Fukada. Prototype of a wire-rope rockfall protective fence developed with three-dimensional numerical modeling. *Computers and Geotechnics*, 54(0):84 – 93, 2013.

[11] Dassault Systémes Simulia Corp, Providence, RI. *Abaqus Analysis User's Manual, Version 6.14*, 2014.

[12] J.O. Hallquist. *LS-DYNA Keyword User's Manual, LS-DYNA R7.1*. Livermore Software and Technology Corporation, Livermore CA, May 2014.

[13] Hans Gerhard Grassl. *Experimentelle und numerische Modellierung des dynamischen Trag- und Verformungsverhaltens von hochflexibeln Schutzsystemen gegen Steinschlag*. PhD thesis, Swiss Federal Institute of Technology, Zurich, 2002.

[14] Axel Volkwein. *Numerische Simulation von flexiblen Steinschlagschutzsystemen*. PhD thesis, Swiss Federal Institute of Technology, Zurich, 2004.

[15] Albrecht Von Boetticher. *Flexible Hangmurenbarrieren: Eine numerische Modellierung des Tragwerks, der Hangmure und der Fluid-Struktur-Interaktion*. PhD thesis, Technische Universitaet Muenchen, 2012.

[16] Leyla GHOUSSOUB, Cyril Douthe, and Karam Sab. Analysis of the mechanical behaviour of soft rockfall barriers. In *RocExs 2014 - 5th Interdisciplinary Workshop on Rockfall Protection*, page 4 p., Italy, May 2014.

[17] Klaus Thoeni, Anna Giacomini, Cédric Lambert, Scott W. Sloan, and John P. Carter. A 3D discrete element modelling approach for rockfall analysis with drapery systems. *International Journal of Rock Mechanics and Mining Sciences*, 68(0):107 – 119, 2014.

[18] J.P. Escallón and C. Wendeler. Numerical simulations of quasi-static and rockfall impact tests of ultra-high strength steel wire-ring nets using abaqus/explicit. In *2013 SIMULIA Community Conference 1 www.3ds.com/simulia*, 2013.

[19] J.P. Escallón, C. Wendeler, and M. Mrozik. Chapter 64. numerical simulation of rock-fall impact on a flexible barrier using abaqus/explicit 6.12. In *Rock Mechanics for Resources, Energy and Environment, Edited by Marek Kwaśniewski and Dariusz Lydżba, CRC Press 2013, Pages 417-423*, 2013.

[20] J.P. Escallón, C. Wendeler, E. Chatzi, and P. Bartelt. Parameter identification of rockfall protection barrier components through an inverse formulation. *Engineering Structures*, 77(0):1 – 16, 2014.

[21] J.P. Escallón, C. Wendeler, E. Chatzi, and P. Bartelt. Mechanics of chain-link wire nets with loose connections. *Engineering Structures*. under review.

[22] Corinna Simone Isabelle Wendeler. *Murgangrueckhalt in Wildbaechen. Grundlagen zu Planung und Berechnung von flexiblen Barrieren von Corinna Simone Isabelle Wendeler*. PhD thesis, ETH, 2008.

[23] W.J. Chung, J.W. Choand, and T. Belytschko. On the dynamic effects of explicit fem in sheet metal forming analysis. *Engineering Computations*, 15 (6):750–776, 1998.

[24] Haipeng Han, Farid Taheri, and Neil Pegg. Quasi-static and dynamic crushing behaviors of aluminum and steel tubes with a cutout. *Thin-Walled Structures*, 45(3):283 – 300, 2007.

[25] Dassault Systémes Simulia Corp, Providence, RI. *Abaqus Analysis User's Manual, Version 6.13*, 2013.

[26] Dassault Systémes Simulia Corp, Providence, RI. *SIMULIA Isight 5.9. User's Guide.*

[27] J.P. Bardet and M.M. Kapuskar. A simplex analysis of slope stability. *Computers and Geotechnics*, 8(4):329 – 348, 1989.

[28] W. Riedel, K. Fischer, C. Kranzer, J. Erskine, R. Cleave, D. Hadden, and M. Romani. Modeling and validation of a wall-window retrofit system under blast loading. *Engineering Structures*, 37(0):235 – 245, 2012.

[29] J. A. Nelder and R. Mead. A simplex method for function minimization. *The Computer Journal*, 7(4):308–313, 1965.

[30] M. D. McKay, R. J. Beckman, and W. J. Conover. Comparison of three methods for selecting values of input variables in the analysis of output from a computer code. *Technometrics*, 21:239–245, 1979.

[31] EOTA. Etag 027 guideline for european technical approval of falling rock protection kits, 2012.

[32] Z. Sternová. European Technical Approval ETA-09/0369. Technical report, TSUS Building Testing and Research Institute, 2010.

[33] S. Przybył and P. Pierański. Helical close packings of ideal ropes. *The European Physical Journal E*, 4(4):445–449, 2001.

[34] O. Sigmund and J. Petersson. Numerical instabilities in topology optimization: A survey on procedures dealing with checkerboards, mesh-dependencies and local minima. *Structural optimization*, 16(1):68–75, 1998.

[35] Andrés Tovar, Neal M. Patel, Glen L. Niebur, Mihir Sen, and John E. Renaud. Topology optimization using a hybrid cellular automaton method with local control rules. *Journal of Mechanical Design*, 128(6):1205–1216, 01 2006.

[36] Heiner Muellerschoen, Andrea Erhart, Krassen Anakiev, Peter Schumacher, and Heribert Kassegger. Application of the equivalent static load method for impact problems with genesis and ls-dyna. In *World congress on structural and multidisc. Optim*, 2013.

[37] Hyun-Ah Lee and Gyung-Jin Park. Nonlinear dynamic response topology optimization using the equivalent static loads method. *Computer Methods in Applied Mechanics and Engineering*, 283(0):956 – 970, 2015.

[38] FE-Design. *TOSCA User's Manual*. FE-Design GmbH, Karlsruhe, Germany, 2008.

[39] Livermore Software Technology Corporation. *LS-TaSC Manual Topology and Shape Computations for LS-DYNA User's Manual*, version 2.0 edition, 2011.

[40] Marta R. Dias, José M. Guedes, Colleen L. Flanagan, Scott J. Hollister, and Paulo R. Fernandes. Optimization of scaffold design for bone tissue engineering: A computational and experimental study. *Medical Engineering & Physics*, 36(4):448 – 457, 2014.

[41] Maggie Kociecki and Hojjat Adeli. Shape optimization of free-form steel space-frame roof structures with complex geometries using evolutionary computing. *Engineering Applications of Artificial Intelligence*, 38(0):168 – 182, 2015.

[42] Guangyong Sun, Guangyao Li, Shiwei Zhou, Hongzhou Li, Shujuan Hou, and Qing Li. Crashworthiness design of vehicle by using multiobjective robust optimization. *Structural and Multidisciplinary Optimization*, 44(1):99–110, 2011.

[43] Jianguang Fang, Yunkai Gao, Guangyong Sun, Chengmin Xu, and Qing Li. Multiobjective robust design optimization of fatigue life for a truck cab. *Reliability Engineering & System Safety*, 135(0):1 – 8, 2015.

[44] Claudio Comis Da Ronco, Rita Ponza, and Ernesto Benini. Aerodynamic shape optimization of aircraft components using an advanced multi-objective evolutionary approach. *Computer Methods in Applied Mechanics and Engineering*, 285(0):255 – 290, 2015.

[45] P. Eberhard. Optimization of mechanical systems. Institute of Engineering and Computational Mechanics Pfaffenwaldring 9, 4th floor 70563 Stuttgart.